Nanoscale

PAPER

View Article Online
View Journal | View Issue



Cite this: *Nanoscale*, 2022, **14**, 5138

# A laser-driven optical atomizer: photothermal generation and transport of zeptoliter-droplets along a carbon nanotube deposited hollow optical fiber†

Hyeonwoo Lee, [a] Mikko Partanen, [a,b] Mingyu Lee,[a] Sunghoon Jeong,[a] Hyeung Joo Lee,[a] Kwanpyo Kim,[c,d] Wonhyoung Ryu, *[e] Kishan Dholakia*[a,f] and Kyunghwan Oh *[a]

From mechanical syringes to electric field-assisted injection devices, precise control of liquid droplet generation has been sought after, and the present state-of-the-art technologies have provided droplets ranging from nanoliter to subpicoliter volume sizes. In this study, we present a new laser-driven method to generate liquid droplets with a zeptoliter volume, breaking the fundamental limits of previous studies. We guided an infrared laser beam through a hollow optical fiber (HOF) with a ring core whose end facet was coated with single-walled carbon nanotubes. The laser light was absorbed by this nanotube film and efficiently generated a highly localized microring heat source. This evaporated the liquid inside the HOF, which rapidly recondensed into zeptoliter droplets in the surrounding air at room temperature. We spectroscopically confirmed the chemical structures of the liquid precursor maintained in the droplets by atomizing dye-dissolved glycerol. Moreover, we explain the fundamental physical principles as well as functionalities of the optical atomizer and perform a detailed characterization of the droplets. Our approach has strong prospects for nanoscale delivery of biochemical substances in minuscule zeptoliter volumes.

Received 21st September 2021,
Accepted 5th March 2022

DOI: 10.1039/d1nr06211e

rsc.li/nanoscale



## Introduction

Controlling the diameter and volume of liquid droplets is a fundamental and critical issue in various areas, such as fluid mechanics, biochemistry, and environmental science.[1–6] In particular, the physical properties of liquid droplets with nanometer-scale maximize their potential to create academic breakthroughs. The rapid development of nanoscience has recently realized this potential, and inducing novel magnetism and specimen preparation for transmitting electronic microscopy are their impactful precedents.[7–10] Furthermore, current airborne plagues have created demands to emulate droplet generation from viscous bioliquids to investigate how the airborne droplets behave.[11–13] Systematic delivery of nano-micro viscous droplets in ambient air can also benefit many interdisciplinary research fields, such as three-dimensional nano printing, advanced molecular synthesis, and drug delivery.[14–18]

In response to these demands, various liquid jetting systems have been developed, where liquid droplets have been ejected and delivered through a nozzle to a target area with droplet diameter/volume distributions artificially controlled by physical impulses.[19–21] These previous approaches commonly require three driving mechanisms: (1) ejection of the liquid, (2) formation of liquid droplets, and (3) delivery of the droplets to the outer environment. Meanwhile, several driving mechanisms, such as ultrasound,[22,23] flow focusing,[24,25] and electrohydrodynamic jetting,[26,27] have been investigated. Nevertheless, they have failed to reach the single liquid droplet volume in the zeptoliter regime, hindering the development of high-resolution nanofluidics. These previous studies have fundamental limits in the relatively large form factor in the nozzle and the requirements of high-energy physical impulses from external sources.[28–30] As an alternative driving mechanism, we have recently investigated the feasibility of controlling the liquid flow using continuous-wave (CW) milliwatt laser light in

[a]*Photonic Device Physics Laboratory, Department of Physics, Yonsei University, 50 Yonsei-ro, Seodaemun-gu, Seoul 03722, Korea. E-mail: koh@yonsei.ac.kr*
[b]*Photonics Group, Department of Electronics and Nanoengineering, Aalto University, P.O. Box 13500, 00076 Aalto, Finland*
[c]*Department of Physics, Yonsei University, Seoul 03722, Korea*
[d]*Center for Nanomedicine, Institute for Basic Science (IBS), Seoul 03722, Korea*
[e]*Biomedical and Energy System Laboratory, Department of Mechanical Engineering, Yonsei University, 50 Yonsei-ro, Seodaemun-gu, Seoul 03722, Korea. E-mail: whryu@yonsei.ac.kr*
[f]*SUPA, School of Physics and Astronomy, University of St Andrews, KY16 9SS, UK. E-mail: kd1@st-andrews.ac.uk*
†Electronic supplementary information (ESI) available. See DOI: 10.1039/d1nr06211e

fiber optic geometry,[31] which generated nanodroplets with a zeptoliter volume scale.

In this study, we propose a novel method called a laser-driven optical atomizer, providing a consistent and repeatable means for droplet generation in a compact all-fiber platform, droplet delivery through the air, and its deposition on a target. We successfully generated liquid droplets whose diameter is in the nanometer range with a single liquid volume scale of zeptoliters. This is the first time such a small volume has been realized on a spray platform. It is well-known that single-walled carbon nanotubes (SWCNTs) work as a perfect light absorber in a wide spectral range from ultraviolet to infrared.[32,33] In this study, we optically deposited SWCNTs at the end of a hollow optical fiber (HOF) with a ring core as a film. We launched a CW infrared laser beam (of milliwatts power) through the HOF. The optical energy of over 90% was absorbed by this carbon nanotube film, efficiently generating a highly localized microring heat source. After launching the laser, the liquid inside the HOF was heated and evaporated, which rapidly recondensed into zeptoliter droplets at room temperature in the air.[34,35] The droplets were delivered over a spherical surface in a well-defined conical geometry over a few hundred micrometers from the end of the HOF. The diameter of the area covered by zeptoliter droplets on a target Si–$SiO_x$ wafer was of the order of a few hundred micrometers, which can be further varied by the distance between the HOF end facet and the wafer, as well as the laser power. Additionally, we confirmed that the chemical composition of the droplets was identical to the bulk liquid precursor by applying spectroscopic analyses, such as fluorescent measurement and Raman spectroscopy. This indicates that the proposed method has excellent prospects for liquid chemical delivery at the nanoscale. The proposed method provides new insight into liquid control physics and droplet manipulation technology. Additionally, the simple all-fiber geometry may enable *in situ* real-time applications in microscopic *in vivo* environments in a minimally invasive manner.[36,37] In the following sections, we describe the physical principles of operation of this all-fiber laser-driven atomizer and discuss the droplet generation and transport characteristics.

## Results and discussion

### Structure and physical mechanism of the optical atomizer

The laser-driven optical atomizer's structure consists of three parts: (1) HOF with a central air hole serving as a liquid reservoir and a high refractive index ring core as a laser waveguide,[38] (2) SWCNTs are deposited on the end facet of HOF serving as a film acting as a microring heater by absorbing laser light, and (3) a fiber-coupled laser diode (LD) emitting at $\lambda$ = 976 nm with a power ranging up to tens of milliwatts. This structure is schematically shown in Fig. 1(a). HOF is fusion spliced to a single-mode fiber (SMF) to adiabatically convert the fundamental mode of SMF to a ring mode of HOF with a low loss.[38] The laser from LD propagates from SMF to HOF,

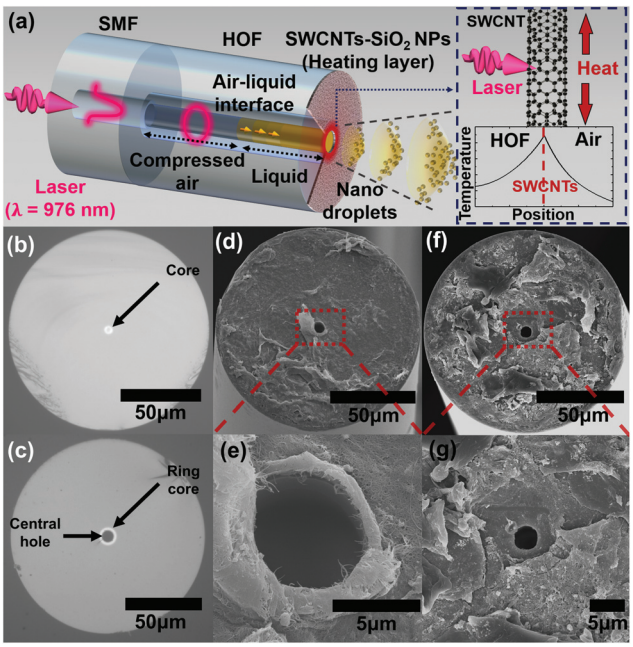


**Fig. 1** (a) Schematic of the optical atomizer. The liquid inside the HOF is vaporized by the photothermal effect of SWCNTs and recondensed to form nanodroplets. The air–liquid interface goes down as the liquid is ejected. The inset represents the temperature distribution as a function of the position nearby the SWCNT–$SiO_2$ NPs layer. Optical microscope image of the end facet of (b) SMF and (c) the HOF. (d) Scanning electron microscope image of the optical atomizer after the optical deposition of SWCNTs and (e) it's magnified image near the central hole. (f) Scanning electron microscope image of the optical atomizer after the optical deposition of $SiO_2$ NPs and (g) it's magnified image near the central hole.

and it is absorbed by carbon nanotube thin film to make a ring-shaped micro-heater. See the right inset of Fig. 1(a).

The liquid glycerol was filled in the central hole of HOF by the capillary force and expelled by a combination of the vapor pressure of the photothermally heated liquid and the air pressure remnant inside the HOF air hole. The droplets from the end facet and air–liquid interface inside HOF were monitored using separate optical microscopes to investigate the droplet transport and liquid dispensation, respectively. The droplets were targeted to a Si–$SiO_x$ wafer at room temperature and collected to investigate the spatial distribution of droplet sizes.

### Fabrication of the all-fiber optical atomizer

Scheme 1 shows that one end of HOF was adiabatically fusion spliced with SMF (Corning HI1060), as presented in Fig. 1(b). The HOF used in this study has a central air hole and ring core outer diameters of 8 and 11 μm, respectively as illustrated in Fig. 1(c). The SMF was connected to LD with a very low loss of less than 1 dB. The other end of HOF was cleaved vertically using an ultrasound cleaver, and the total HOF length in the atomizer was approximately 5 mm. The cleaved end was immersed in an SWCNT colloidal suspension (Sigma-Aldrich,

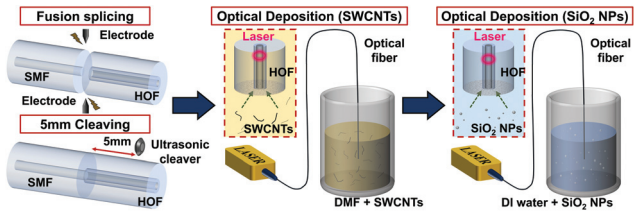


**Scheme 1** Fabrication process of the optical atomizer.

Cat. No. 805033). The concentration was 0.17 g $L^{-1}$ in dimethylformamide (Sigma-Aldrich), and the ultrasonic homogenizer dispersed SWCNTs. Approximately 100 mW laser was launched into the core of the optical fibers for an hour while keeping the HOF inside the solution. SWCNT flakes were deposited near the ring core at the end facet by the optical gradient force, consistent with the previously reported optical deposition of SWCNTs on an optical fiber.[39,40] Fig. 1(d, e) show the scanning electron microscope (SEM) images of the prepared fiber facet. Over the SWCNT thin film, we subsequently deposited $SiO_2$ nanoparticles ($SiO_2$ NPs, PlasmaChem GmbH) with an average diameter of 20 nm to reduce the hydrophobicity of the SWCNT deposited surface.[41–44] We immersed the prepared fiber facet into $SiO_2$ nanoparticle colloidal suspension. $SiO_2$ particles were loaded approximately 17 mg $L^{-1}$ in deionized water. We also launched a laser of approximately 500 μW to HOF for 5 s. This process is necessary to facilitate the liquid filling into HOF since hydrophobic SWCNT film competes with the capillary force, repelling the liquid from the HOF end face.[41–44] Fig. 1(f and g) show the SEM image of the optical atomizer after $SiO_2$ NPs deposition. The laser light absorption $A$ through the prepared SWCNT deposited HOF was approximately 93%, providing an efficient photothermal conversion. The thickness of SWCNT thin film $z_{SWCNTs}$ was estimated as 60 nm using the reported SWCNT absorption coefficient $\alpha$ of approximately $4.2 \times 10^5$ $cm^{-1}$ and eqn (1), which is derived from the Beer–Lambert law.[33,45–47]

$$A = (1 - \exp(-\alpha z_{SWCNTs})). \quad (1)$$

We filled the prepared HOF tip using the capillary force by dipping HOF into the liquid reservoir. The volume of a liquid filled inside the fiber is only a few hundred picoliters. A liquid with a high vapor pressure of more than 0.004 kPa at 25 °C, such as water or alcohol, rapidly evaporates within a few seconds at a normal humidity of approximately 40%.[48,49] Appropriate chemicals may be added to decrease the vapor pressure of these liquids. We successfully atomized low vapor pressure viscous liquids, such as oleic acid and triethylene glycol. Details of these studies will be described in a separate paper.[50,51] In this paper, we specifically chose glycerol with a high viscosity, causing technical challenges in previous atomizers despite its various potential applications in biochemical technologies.[52–54] Note that HOF was not completely filled by glycerol, but air with a volume of approximately 238 pl remained inside, providing approximately 5.5 kPa outward pressure to the liquid. This pressure is attributed to one of the main driving forces to eject and deliver the droplets.

## Liquid droplet generation and transport in the all-fiber optical atomizer

We discovered that two air–liquid interfaces were created inside the HOF at the inner part (called interface-1) and at the end facet of the fiber (called interface-2). These served as good functional indicators of our optical atomizer. Fig. 2(a) shows that the two interfaces behaved predictably for an absorbed laser power of less than 20 mW. To examine the capability of the optical atomizer, we used a bright-field optical microscope to monitor interface-1. The image sensor was synchronized with the LD driver to start the video recording simultaneously with the laser irradiation. We varied the absorbed laser power from 0 to 19 mW. We used another optical microscope near the end facet to observe interface-2 and droplet generation from HOF and its transport in air.

Consequently, we obtained that the proposed optical atomizer required a certain amount of laser power for the operation to heat the glycerol above its evaporation temperature. Specifically, to eject the liquid inside the HOF, the SWCNT heater must induce a vapor pressure $P_{vapor}$ exceeding the pressure $P_{capillary}$ of the air–liquid interface-2. We define such a moment as the ejection initiating time $t_i$. Here the Laplace–Young equation can express $P_{capillary}$, which is a function of the hole radius $R_{hole}$ of HOF, surface tension of the liquid $\sigma$, and contact angle of liquid $\theta$ inside the capillary, as shown in eqn (2).[55]

$$P_{capillary} = 2\sigma\cos\theta/R_{hole} < P_{vapor}(t_i). \quad (2)$$

Theoretical analysis with solutions of the heat equation is provided in ESI.† Experimentally, there existed a temporal

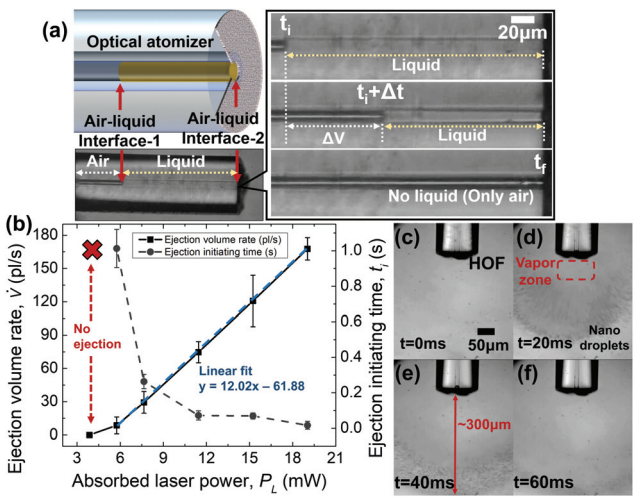


**Fig. 2** (a) Air–liquid interfaces for measuring optofluidic properties of the optical atomizer. The enlarged bright-field microscope image shows the liquid filled inside the capillary of HOF. (b) The ejection volume rate and ejection initiating time as a function of the laser power absorbed by the SWCNT thin film. (c–f) The nanodroplets from the atomizer were recorded using a high-speed camera. The absorbed laser power is 19 mW.

delay, which was the liquid ejection initiating time, between the liquid atomization and laser onset. By carefully analyzing the frames taken by the computational metal–oxide semiconductor (CMOS) camera on the optical microscope and monitoring the air–liquid interface-1, we measured the liquid ejection initiating time and the ejection volume rate as a function of the absorbed laser power at the SWCNT film on the HOF end facet. Fig. 2(b) summarizes the details.

Moreover, we performed laser irradiation for 0.1–2.5 s and observed that interface-1 did not shift until the absorbed laser power reached 5.76 mW. The liquid ejection time required in the optical atomizer was measured for various absorbed laser powers. The results are summarized as solid circles in Fig. 2(b). The liquid ejection initiating time rapidly decreased from 1 second to less than 300 ms as the laser power increased above 7 mW.

For an absorbed laser power ranging from 5.76 to 19.0 mW, we consistently observed that interface-1 shifted toward the HOF end facet (Fig. 2(a)). The initial liquid-air interface at $t = t_i$ is shown above, and the interface at $t = t_f$ when the laser is turned off. Here, the darker area denotes the air (refractive index $n = 1$), and glycerol ($n = 1.46$) was not distinguishable from the silica ($n = 1.45$) of HOF using the bright-field optical microscope.

In this absorbed laser power range, interface-1 shifted toward the end facet on the right-hand side, whereas interface-2 remained at its initial position. Thus, the shift of the interface-1 directly represents the volume of the liquid ejected out of the HOF in this laser power range. The liquid ejection volume rate ($\dot{V}$), defined as the volume difference of glycerol between the ejection initiating time ($t_i$) and the end of the liquid atomization ($t_f$), was experimentally measured for various laser power. Fig. 2(b) summarizes the details. We obtained that $\dot{V}$ and the absorbed laser power were linearly correlated with regression parameters of 12.0 pl (s mW)$^{-1}$. Based on these observations, the liquid ejection volume ($V$) during an arbitrary time $t(t_i < t < t_f)$, at the given absorbed laser power ($P_L$), $t_i$, and $t_f$, is well-approximated as follows:

$$V = \dot{V}(P_L, t_i, t_f)(t - t_i). \quad (3)$$

Note that $\dot{V}$ can be flexibly controlled from the minimum value of 8.61 pl s$^{-1}$ for the laser power of 5.76 mW to the maximum value of 168 pl s$^{-1}$ for the absorbed laser power of 19.0 mW. Note that $t_i$ and $t_f$ varied with the absorbed laser power. Table 1 summarizes the details. From the experimental observation in Fig. 2(b), we estimated the mass flow of 211 ng s$^{-1}$ using the proposed optical atomizer by multiplying the density of glycerol of 1.26 g ml$^{-1}$, which is several orders of magnitude lower than previous atomizers,[56–58] to numerically analyze the behavior of the droplets, as shown in Fig. S1 (ESI).†

We used another optical microscope to observe the droplet generation and its transport in the air near the film deposited end facet of HOF.

In Fig. 2(c–f), the frames are shown sequentially for the absorbed laser power of 19 mW. The droplet recondensation in the ambient air was insufficient to be observed by the microscope at lower power. In Fig. 2(c), we observed the air–liquid interface near the SWCNT deposited end facet at $t$ = 0 ms. Meanwhile, at $t$ = 20 ms, which is close to $t_i$, we observed observe nanodroplets with a zeptoliter volume scale exhumed from HOF. It is worth noting that the droplets with different sizes were formed at a certain distance away from the HOF end facet. We also observed a region where liquid droplets were not observed, and only vapor existed. See the "vapor zone" in Fig. 2(d). The "vapor zone" extended to 60 μm from the end facet. Beyond this zone, glycerol started recondensation to form nanodroplets with a zeptoliter volume scale. In the subsequent frame at $t$ = 40 ms, we observed the typical transport pattern of the optical atomizer such that all droplets were distributed on a spherical surface in the air, whose lateral boundary had a conical shape. Its maximum radius was approximately 300 μm, and the conical angle was approximately 29°.

This unique trajectory of the droplet is because of the convective flow of the ambient air induced by the nanotube film heater. It is numerically demonstrated in Movie S1–3 and Fig. S1 (ESI).† Additionally, we investigated the droplet size/volume dependence on their longitudinal distance using a finite element method package, COMSOL. The details of the corresponding results are summarized in Fig. S2 of ESI.† Furthermore, droplets propagated toward a target wafer, and their size distribution was statistically analyzed as described in the following sections.

### Droplet size distribution measured by cryogenic SEM

To characterize droplets from the proposed optical atomizer, we collected them on a Si–SiO$_x$ wafer, as shown in Fig. 3(a). Here, the atomizer was vertically placed 40 μm away from the wafer, and the absorbed laser power was 9 mW with an irradiation time of approximately 100 ms. We used a cryogenic SEM (cryo-SEM)[59] freezing the droplets at liquid nitrogen temperature (under 77 K) immediately after they were deposited on the wafer. The frozen glycerol droplets prevented evaporation in a high vacuum experimental condition in the SEM chamber. The frost undesirably formed on the sample was removed *via* sublimation, adjusting the temperature and atmospheric pressure inside the cryo-SEM chamber.

**Table 1** Temporal response of optical atomizer depending on laser power

| Absorbed laser power (mW) | 5.76 | 7.65 | 11.4 | 15.2 | 19.0 |
|---|---|---|---|---|---|
| $t_i$ (s) | $1.01 \times 10^{0}$ | $2.63 \times 10^{-1}$ | $7.23 \times 10^{-2}$ | $6.93 \times 10^{-2}$ | $1.66 \times 10^{-2}$ |
| $t_f$ (s) | $2.33 \times 10^{0}$ | $6.50 \times 10^{-1}$ | $2.24 \times 10^{-1}$ | $1.63 \times 10^{-1}$ | $8.40 \times 10^{-2}$ |

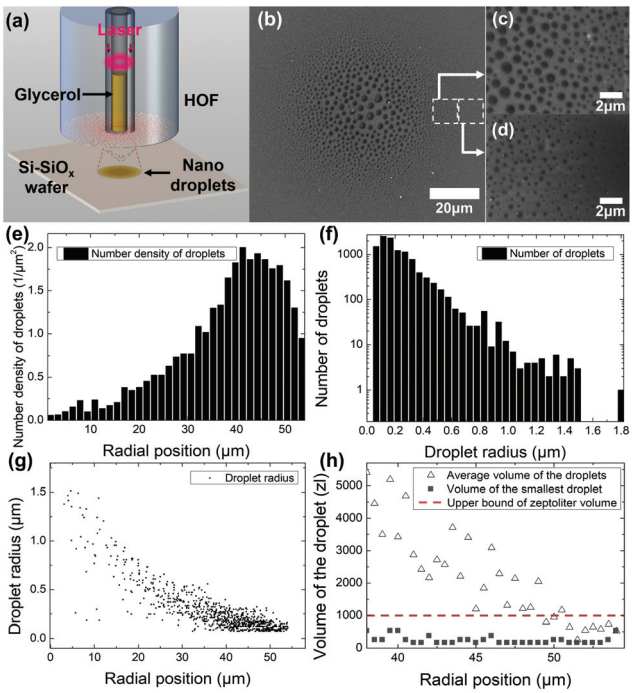


**Fig. 3** (a) Schematic of the preparation process of a specimen for characterizing the droplet size. (b) The cryo-SEM image of the glycerol droplets and (c and d) its magnified images. (e) The number density of the droplets as a function of the radial position. (f) The number of droplets as a function of the droplet radius. (g) The droplet radius as a function of the radial position. (h) The average volume of the droplets and the volume of the smallest droplet as a function of the radial position. Below the red dotted line are the droplets with a zeptoliter volume scale, and above it are attoliter droplets.

Images taken from the cryo-SEM are shown in Fig. 3(b–d), illustrating a unique spatial distribution. In the vicinity of the optical atomizer axis, we observed significantly larger droplets at the center of Fig. 3(b). This is attributed to the coalescence of multiple droplets.[60,61] As the liquid inside HOF is atomized, its gas molecules diffuse in the air and condense into droplets as they reach the substrate. In terms of statistical mechanics, only a few gas molecules can reach far from the fiber axis, requiring a high radial velocity and long diffusion distance.[62] For this reason, several nanodroplets with a zeptoliter volume scale are separately deposited at the edge. However, since most gas molecules exist in a high concentration near the central axis, several nanodroplets are generated and are in contact with one another.[62,63] As shown in a cryo-SEM image, their contact coalesces into large microdroplets near the center.[63,64] Consequently, the diameter of the droplets decreased as its position moved radially outward where droplets had rarely coalesced. We magnified the image of droplets in two regions whose radial positions were 40 and 50 μm, as shown in Fig. 3(c and d), respectively. These figures show that the proposed atomizer generated nanodroplets with a zeptoliter volume scale. We used an image recognition routine in MATLAB to collect information on the spatial distribution of droplet size along the horizontal axis of the cryo-SEM image.

Fig. 3(e) shows the number density of droplets per unit area as a function of the radial position referenced from the center. Here, we obtained that an order of larger number of droplets 1.5–2.0 $\mu m^{-2}$ was deposited in the peripheral (radial position in the range of 40–50 μm) than 0.1–0.3 $\mu m^{-2}$ near the center. In Fig. 3(f), we obtained that nanodroplets with a zeptoliter volume scale outnumbered micron diameter droplets with a femtoliter volume scale by several orders of magnitude, strongly indicating that the proposed optical atomizer generated nanodroplets with a zeptoliter volume scale. Glycerol droplets with a radius of approximately 74 nm showed more than 1000 counts in the figure, and their volume corresponded to 156 zl. In this volume calculation, we assumed that they have spherical cap shapes. The contact angle of the bulk glycerol and Si–$SiO_x$ wafer was experimentally evaluated as 51° using a conventional method based on a digital camera.[65,66] Thus, to investigate the volume of relatively less coalesced droplets, we calculated the average and minimum volume as a function of a radial position with 38–54 μm domain, as shown in Fig. 3(h). The average volume of the droplets increases monotonically as the radial position gets closer to the center since the number of coalesced droplets increases. Nevertheless, the minimum volume of the droplet was consistent in the zeptoliter scale, demonstrating that most of the large droplets imaged by cryo-SEM are because of coalescing of the nanodroplets with a zeptoliter volume scale. To the best of our knowledge, this volume is the smallest observed in liquid atomizing technology. Fig. 3(g) shows the droplet size distribution as a function of the radial position, where the droplet radius monotonically decreased from a few micrometers to tens of nanometers as the radial position increased.[67,68]

## Comparison of chemical structures of bulk liquid and atomized liquid nanodroplets

It would be highly beneficial if the chemical composition of the liquid could be maintained through the laser-driven atomization process. This means that the physical and chemical properties of the bulk liquid can be transferred to the nanodroplets, which can open up a new avenue for nanoscopic chemical delivery applications. In this study, we applied micro-Raman spectroscopy (LabRAM ARAMIS, HORIBA Jobin Yvon Raman Division) and fluorescence measurements (HR4000, Ocean Optics) to investigate the chemical structure of the liquid droplets sprayed using the proposed optical atomizer and compared the data with that of the original bulk liquid.

First, we used glycerol without any chemical additives and set the optical atomizer similarly to those of Fig. 3(a). To obtain a sufficiently high Raman scattering signal from the droplets, we extended the irradiation time to 1 s, increasing the central drop diameter to approximately 100 μm. Note that the large central droplet was formed by coalescing individual nanodroplets with a zeptoliter volume scale, and it can represent their chemical properties. A bulk glycerol droplet was also formed on the same wafer using the micropipette with a diameter of approximately 1 mm. Fig. 4(a) summarizes the Raman spectra of the atomized droplet, bulk glycerol, and

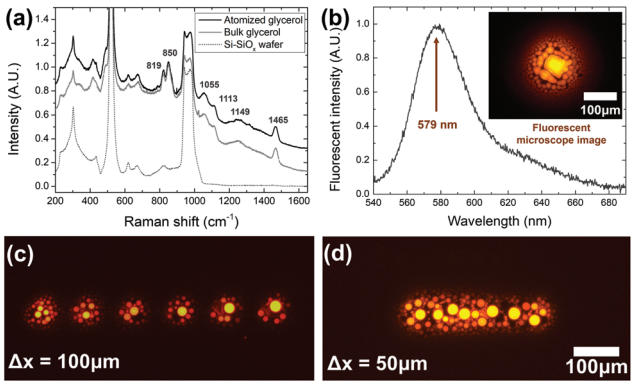


**Fig. 4** (a) Raman spectra of the Si–$SiO_x$ wafer, atomized, and bulk glycerol from the optical atomizer. (b) The fluorescent spectrum of the atomized glycerol-rhodamine B solution with 3 g $L^{-1}$ concentration. The inset shows the fluorescent microscope image. Fluorescent microscope image of the six shots of the atomized glycerol-rhodamine B solution with consistent interval $\Delta x$ of (c) 100 μm and (d) 50 μm.

wafer. Unique Raman signatures of glycerol liquid[69] were clearly observed for both liquid samples to confirm that the chemical structures were maintained through the proposed optical atomization process.

Moreover, we investigated the chemical delivery capability of the proposed optical atomizer by dissolving a fluorescent dye in the glycerol. We prepared a glycerol solution with a rhodamine B concentration of 3 g $L^{-1}$. Consequently, droplets were generated by the proposed optical atomizer with an absorbed laser power of 15 mW and a laser irradiation time of 200 ms. A pump laser at $\lambda$ = 532 nm was focused near the central droplet, and the fluorescence from the dye-doped glycerol droplet was observed through a fluorescent microscope (IX71, Olympus), as shown in the inset of Fig. 4(b). The emission from the central droplet was collected, and its spectrum is shown in Fig. 4(b). A peak at 579 nm with a full width at half maximum of 40 nm was observed, which is highly consistent with the emission characteristics of rhodamine B.[70]

We also demonstrated that the optical atomizer can highly repeatable multiple ejections with glycerol-rhodamine B solution. Based on the experimental setup similar to Fig. 3(a), where the HOF was placed 30 μm above the wafer, absorbed laser power was 19 mW, and irradiation time was 27.5 ms. After single atomization, the optical atomizer was translated by a constant interval $\Delta x$. This operation was repeated six times. Fig. 4(c) shows that the distinguishable and uniform marks of six times of atomization were observed through a fluorescent microscope for $\Delta x$ = 100 μm. This result shows that multiple atomization processes can be consistently conducted using the dye-dissolved glycerol. Furthermore, once the interval was decreased to $\Delta x$ = 50 μm, the microscope confirmed a line was formed on the wafer where the individual shots were not distinguishable, as shown in Fig. 4(d).

The experimental confirmation in Fig. 4 strongly indicates that the proposed optical atomizer can effectively deliver the chemical and physical properties of a bulk liquid to nanodroplets with a zeptoliter volume scale. Additionally, transporting dye-dissolved solutions is highly expectable and repeatable, which can initiate new metrology for micro–nanoscopic drug delivery.

## Discussions

The proposed all-fiber optical atomizer was compared with previous technologies (see Table 2) in terms of the operation principle, driving source, liquid properties, liquid volume, droplet volume, and physical size. In this comparison, the all-fiber optical atomizer uses the least amount of energy (<20 mJ), <20 mW CW laser irradiation for <1 s. These represent more moderate experimental conditions than previous technologies that require a few hundred-kilowatts pulsed laser and kilovolt scale electric potential. This results in a moderate speed of droplets of a few centimeters per second, whereas several other techniques produce higher velocities at the meter-per-second order.

**Table 2** Comparison of the proposed optical atomizer with previous technologies

| Principle | Driving source | Liquid | Liquid viscosity | Liquid volume per shot | Single droplet volume | Hole/outer diameter of nozzle | Speed of droplets |
|---|---|---|---|---|---|---|---|
| Photothermal effect (this work) | <20 mW CW laser diode | Glycerol | 1412 mPa·s | 9 pl | ~156 zl | 8 μm/125 μm | ~1 cm $s^{-1}$ |
| Laser induced cavitation (ref. 71) | ~300 kW Nd-YAG nanosecond laser | Glycerol-water mixture | 100 mPa·s | 10 nl | N.A. | 150 μm/3 mm | ~100 m $s^{-1}$ |
| coulombic force (ref. 56) | ~1.6 kV electric potential | Water | 0.89 mPa·s | 40 nl | ~1 fl | 42 μm/85 μm | N.A. |
| Air blast (ref. 57) | Multiphase flow | Glycerol-water mixture | ~6 mPa·s | 5 ml | N.A. | 2 mm/4 mm | ~5 m $s^{-1}$ |
| Air blast (ref. 72) | Multiphase flow | Glycerol-water mixture | 259 mPa·s | N.A. | ~5 pl | 0.41 mm/ ~1.3 cm | N.A. |
| Ultrasound atomization (ref. 73) | ~3 W acoustic wave | Water | 0.89 mPa·s | ~10 μl | ~1 pl | 130 μm/ 1.24 mm | ~19 mm $s^{-1}$ |
| Pressure from a Piezo actuator (ref. 58) | Piezoelectric disk | Water | 0.89 mPa·s | 5 μl | N.A. | 8 μm/10 mm | N.A. |

This low energy requirement enables the proposed optical atomizer to easily deliver viscous liquids to fragile targets, such as soft tissue, biological samples, and flexible organic substrates. Furthermore, the volume control of the ejected liquid from the atomizer (a few picoliters per shot) and the single droplet volume of a few hundred zeptoliters are the smallest to date. The proposed device consists of only a single strand of fiber with a cladding and hole diameters of 125 and 8 μm, respectively, providing the smallest form factor and enabling real-time, *in situ* liquid ejections in a microscopic environment, which was not possible in previous technologies. This enables optical atomizers to deposit liquids in a highly localized area, as shown in Fig. 2(c–f) and 3(b), in contrast to traditional spray platforms that only target macroscopic objects over 1 mm. In terms of chemical capability, previous studies of liquid atomization (see Table 2) demonstrated the delivery of various materials dissolved in the liquid. For example, some previous studies implemented human tissue mimicry by depositing polymer materials,[20,74] precision printing using colored inks,[75,76] and drug delivery with therapeutic molecules.[17,18] In this study, we also confirmed that an optical atomizer could dissolve and eject a fluorescent dye, rhodamine B, at a much smaller scale than other technologies. This suggests that the proposed optical atomizer technology can be used for other various chemical applications based on these previous studies. Furthermore, multiple ejections of the dye-dissolved glycerol can be achieved using this device for a unique spray patterning process, indicating a high potential to be a strong alternative to the current spray printing equipment and conventional single droplet inkjet technologies.[77–80]

## Conclusion

In this study, we have successfully explored a new application of SWCNTs integrated with a HOF to convert bulk liquid into nanodroplets with a zeptoliter volume scale using a monolithic optical fiber solution. By inducing the photothermal generation on the carbon nanotube thin film with tens of milliwatt CW laser, the glycerol filled inside the central hole of HOF was evaporated and recondensed to be transported approximately 300 μm longitudinal distance. The nanoscopic morphology of the nanodroplets with a zeptoliter volume scale was confirmed by employing cryo-SEM. We confirmed that its chemical structure was preserved through Raman spectroscopy and fluorescent measurement. As a potential application, we could deliver dye-dissolved liquid so that glycerol-rhodamine B solution preserved its unique fluorescent characteristic after the atomization. The proposed device was demonstrated to be used for the patterning process of dye-dissolved liquid. Hence, this technology uses fiber optic components to form zeptoliter viscous droplets, as a powerful solution for highly localized targets, beyond the spatial limit of the conventional liquid spray methodologies. With a microscopic feature, low energy requirement, and high volumetric precision, the approach will enable advanced *in vivo* applications and future patterning technologies.

## Author contributions

H. Lee conceived the idea and designed and performed the experiments and simulations. H. Lee wrote the manuscript. M. Partanen figured out the principle of this device and analyzed the cryo-SEM data. M. Lee, S. Jeong, and H. J. Lee conducted helpful discussions and arranged the references. K. Kim advised about the nanodroplets characterization. W. Ryu, K. Dholakia, and K. Oh acquired funding, supervised this study, and critically reviewed/edited the manuscript.

## Conflicts of interest

There are no conflicts to declare.

## Acknowledgements

This work was supported by the National Research Foundation of Korea (NRF) grant by the Korea government (MSIT) (No. 2019R1A2C2011293) and University of Sydney – Yonsei University Partnership Collaboration Awards. M. P. acknowledges European Union's Horizon 2020 Marie Sklodowska-Curie Actions (MSCA) individual fellowship under Contract No. 846218. KD thanks the UK Engineering and Physical Sciences Research Council for funding (grant EP/P030017/1). H. Lee thanks Dr Yangjin Lee, Mr Jun-Yeong Yoon, and Mr Joong-Eon Jung for helpful discussion.

## References

1 M. L. Kovarik and S. C. Jacobson, *Anal. Chem.*, 2007, **79**, 1655–1660.
2 E. Ko, J. S. Lee, H. Kim, S. Y. Yang, D. Yang, K. Yang, J. Lee, J. Shin, H. S. Yang, W. Ryu and S. W. Cho, *ACS Appl. Mater. Interfaces*, 2018, **10**, 7614–7625.
3 P. Cadinu, B. P. Nadappuram, D. J. Lee, J. Y. Y. Sze, G. Campolo, Y. Zhang, A. Shevchuk, S. Ladame, T. Albrecht, Y. Korchev, A. P. Ivanov and J. B. Edel, *Nano Lett.*, 2017, **17**, 6376–6384.
4 B. K. Kim, J. Kim and A. J. Bard, *J. Am. Chem. Soc.*, 2015, **137**, 2343–2349.
5 S. I. Kim, Y. J. Kim, H. Hong, J. H. Yun and W. H. Ryu, *ACS Appl. Mater. Interfaces*, 2020, **12**, 54683–54693.
6 S. H. Eom, S. Senthilarasu, P. Uthirakumar, S. C. Yoon, J. Lim, C. Lee, H. S. Lim, J. Lee and S. H. Lee, *Org. Electron.*, 2009, **10**, 536–542.
7 S. Chung, Q. T. Le, M. Ahlberg, A. A. Awad, M. Weigand, I. Bykova, R. Khymyn, M. Dvornik, H. Mazraati, A. Houshang, S. Jiang, T. N. A. Nguyen, E. Goering,

 

G. Schutz, J. Grafe and J. Akerman, *Phys. Rev. Lett.*, 2018, **120**, 217204.
8 Z. Lecz and A. Andreev, *Phys. Rev. Res.*, 2020, **2**, 023088.
9 J. M. Yuk, J. Park, P. Ercius, K. Kim, D. J. Hellebusch, M. F. Crommie, J. Y. Lee, A. Zettl and A. P. Alivisatos, *Science*, 2012, **336**, 61–64.
10 Q. Chen, J. M. Smith, J. Park, K. Kim, D. Ho, H. I. Rasool, A. Zettl and A. P. Alivisatos, *Nano Lett.*, 2013, **13**, 4556–4561.
11 M. P. Atkinson and L. M. Wein, *Bull. Math. Biol.*, 2008, **70**, 820–867.
12 G. Buonanno, L. Stabile and L. Morawska, *Environ. Int.*, 2020, **141**, 105794.
13 W. G. Lindsley, T. A. Pearce, J. B. Hudnall, K. A. Davis, S. M. Davis, M. A. Fisher, R. Khakoo, J. E. Palmer, K. E. Clark, I. Celik, C. C. Coffey, F. M. Blachere and D. H. Beezhold, *J. Occup. Environ. Hyg.*, 2012, **9**, 443–449.
14 Y. W. Han and J. Y. Dong, *J. Micro Nano-Manuf.*, 2018, **6**, 040802.
15 S. Aphinyan, E. Y. M. Ang, J. J. Yeo, T. Y. Ng, R. M. Lin, Z. S. Liu and K. R. Geethalakshmi, *Modell. Simul. Mater. Sci. Eng.*, 2019, **27**, 055005.
16 H. G. Nie, Z. W. Wei, L. Q. Qiu, X. S. Chen, D. T. Holden and R. G. Cooks, *Chem. Sci.*, 2020, **11**, 2356–2361.
17 Y. Cao, Y. L. Chen, T. Yu, Y. Guo, F. Q. Liu, Y. Z. Yao, P. Li, D. Wang, Z. G. Wang, Y. Chen and H. T. Ran, *Theranostics*, 2018, **8**, 1327–1339.
18 N. Rapoport, *Adv. Exp. Med. Biol.*, 2016, **880**, 221–241.
19 O. J. Jaber, A. Kourmatzis and A. R. Masri, *Energy Fuels*, 2021, **35**, 7144–7155.
20 S. Y. Yang, T. H. Hwang, L. Che, J. S. Oh, Y. Ha and W. Ryu, *Biomed. Mater.*, 2015, **10**, 035011.
21 M. Cloupeau and B. Prunetfoch, *J. Aerosol Sci.*, 1994, **25**, 1021–1036.
22 B. Avvaru, M. N. Patil, P. R. Gogate and A. B. Pandit, *Ultrasonics*, 2006, **44**, 146–158.
23 A. Dalmoro, A. A. Barba, G. Lamberti and M. d'Amore, *Eur. J. Pharm. Biopharm.*, 2012, **80**, 471–477.
24 A. M. Ganan-Calvo, *Appl. Phys. Lett.*, 2005, **86**, 214101.
25 J. M. Parrilla-Gutierrez, S. Tsuda, J. Grizou, J. Taylor, A. Henson and L. Cronin, *Nat. Commun.*, 2017, **8**, 1–9.
26 S. P. Zhang, J. Lata, C. Y. Chen, J. Mai, F. Guo, Z. H. Tian, L. Q. Ren, Z. M. Mao, P. H. Huang, P. Li, S. J. Yang and T. J. Huang, *Nat. Commun.*, 2018, **9**, 1–11.
27 M. S. Onses, C. Song, L. Williamson, E. Sutanto, P. M. Ferreira, A. G. Alleyne, P. F. Nealey, H. Ahn and J. A. Rogers, *Nat. Nanotechnol.*, 2013, **8**, 667–675.
28 B. Bessaire, M. Mathieu, V. Salles, T. Yeghoyan, C. Celle, J. P. Simonato and A. Brioude, *ACS Appl. Mater. Interfaces*, 2017, **9**, 950–957.
29 L. Rodriguez, N. Passerini, C. Cavallari, M. Cini, P. Sancin and A. Fini, *Int. J. Pharm.*, 1999, **183**, 133–143.
30 J. Rosell-Llompart and A. M. Ganan-Calvo, *Phys. Rev. E: Stat., Nonlinear, Soft Matter Phys.*, 2008, **77**, 036321.
31 H. Choi, M. Park, D. S. Elliott and K. Oh, *Phys. Rev. A*, 2017, **95**, 053817.
32 C. J. Chen, Y. J. Li, J. W. Song, Z. Yang, Y. Kuang, E. Hitz, C. Jia, A. Gong, F. Jiang, J. Y. Zhu, B. Yang, J. Xie and L. B. Hu, *Adv. Mater.*, 2017, **29**, 1701756.
33 Z. Yin, H. M. Wang, M. Q. Jian, Y. S. Li, K. L. Xia, M. C. Zhang, C. Y. Wang, Q. Wang, M. Ma, Q. S. Zheng and Y. Y. Zhang, *ACS Appl. Mater. Interfaces*, 2017, **9**, 28596–28603.
34 H. Zhao and D. Beysens, *Langmuir*, 1995, **11**, 627–634.
35 R. Marek and J. Straub, *Int. J. Heat Mass Transfer*, 2001, **44**, 39–53.
36 J. A. Guggenheim, J. Li, T. J. Allen, R. J. Colchester, S. Noimark, O. Ogunlade, I. P. Parkin, I. Papakonstantinou, A. E. Desjardins, E. Z. Zhang and P. C. Beard, *Nat. Photonics*, 2017, **11**, 714–719.
37 I. T. Leite, S. Turtaev, X. Jiang, M. Siler, A. Cuschieri, P. S. Russell and T. Cizmar, *Nat. Photonics*, 2018, **12**, 33–39.
38 K. W. Oh, S. Choi, Y. M. Jung and J. W. Lee, *J. Lightwave Technol.*, 2005, **23**, 524–532.
39 A. Martinez, K. Fuse, B. Xu and S. Yamashita, *Opt. Express*, 2010, **18**, 23054–23061.
40 J. W. Nicholson, R. S. Windeler and D. J. DiGiovanni, *Opt. Express*, 2007, **15**, 9176–9183.
41 F. F. Chen, Y. Jia, Q. G. Wang, X. B. Cao, Y. H. Li, Y. Lin, X. Cui and J. Q. Wei, *Carbon*, 2018, **137**, 88–92.
42 Y. J. Mao, C. L. Chen and Y. W. Zhang, *Appl. Phys. A: Mater. Sci. Process.*, 2013, **111**, 747–754.
43 S. Iglauer, A. Salamah, M. Sarmadivaleh, K. Y. Liu and C. Phan, *Int. J. Greenhouse Gas Control*, 2014, **22**, 325–328.
44 U. B. Singh, R. P. Yadav, R. K. Pandey, D. C. Agarwal, C. Pannu and A. K. Mittal, *J. Phys. Chem. C*, 2016, **120**, 5755–5763.
45 F. De Nicola, C. Pintossi, F. Nanni, I. Cacciotti, M. Scarselli, G. Drera, S. Pagliara, L. Sangaletti, M. De Crescenzi and P. Castrucci, *Carbon*, 2015, **95**, 28–33.
46 D. F. Swinhart, *J. Chem. Educ.*, 1962, **39**, 333–335.
47 T. G. Mayerhöfer, H. Mutschke and J. Popp, *ChemPhysChem*, 2016, **17**, 1948–1955.
48 V. Nedela, E. Tihlarikova and J. Hrib, *Microsc. Res. Tech.*, 2015, **78**, 13–21.
49 B. Tabah, I. N. Pulidindi, V. R. Chitturi, L. M. R. Arava, A. Varvak, E. Foran and A. Gedanken, *J. Mater. Chem. A*, 2017, **5**, 15486–15506.
50 F. Gironi, M. Maschietti and V. Piemonte, *Energy Sources, Part A*, 2010, **32**, 1861–1868.
51 F. Meyer, R. Eggers, K. Oehlke, B. Harbaum-Piayda, K. Schwarz and M. A. Siddiqi, *Eur. J. Lipid Sci. Technol.*, 2011, **113**, 1363–1374.
52 D. F. Pisani, C. D. K. Bottema, C. Butori, C. Dani and C. A. Dechesne, *Biochem. Biophys. Res. Commun.*, 2010, **396**, 767–773.
53 R. Ciriminna and M. Pagliaro, *Adv. Synth. Catal.*, 2003, **345**, 383–388.
54 A. D. Hocking and J. I. Pitt, *Appl. Environ. Microbiol.*, 1980, **39**, 488–492.
55 D. B. Asay, M. P. de Boer and S. H. Kim, *J. Adhes. Sci. Technol.*, 2010, **24**, 2363–2382.

56 J. H. Jeong, H. Choi, K. Park, H. Kim, J. Choi, I. Park and S. S. Lee, *Polymer*, 2020, **194**, 122405.
57 Z. Feichi, Z. Thorsten, M. Thomas, W. Simon, J. Tobias, H. Peter, Z. Nikolaos, T. Dimosthenis and K. Thomas, *Renewable Sustainable Energy Rev.*, 2020, **134**, 110411.
58 Y. Y. Feng, Z. Y. Zhou, J. H. Zhu and G. B. Du, *Acta Mech. Sin.*, 2007, **23**, 163–172.
59 H. J. Ensikat, A. J. Schulte, K. Koch and W. Barthlott, *Langmuir*, 2009, **25**, 13077–13083.
60 G. F. Christopher, J. Bergstein, N. B. End, M. Poon, C. Nguyen and S. L. Anna, *Lab Chip*, 2009, **9**, 1102–1109.
61 F. Shen, Y. Li, Z. M. Liu, R. T. Cao and G. R. Wang, *Chin. J. Anal. Chem.*, 2015, **43**, 1942–1954.
62 S. J. Blundell and K. M. Blundell, *Concepts in thermal physics*, Oxford University Press on Demand, 2010.
63 J. E. Castillo and J. A. Weibel, *Int. J. Heat Mass Transfer*, 2018, **118**, 708–719.
64 J. R. Castrejon-Pita, E. S. Betton, K. J. Kubiak, M. C. T. Wilson and I. M. Hutchings, *Biomicrofluidics*, 2011, **5**, 014112.
65 Z. A. Zhou, H. Hussein, Z. H. Xu, J. Czarnecki and J. H. Masliyah, *J. Colloid Interface Sci.*, 1998, **204**, 342–349.
66 V. Fernandez and M. Khayet, *Front. Plant Sci.*, 2015, **6**, 510.
67 L. A. Alvarez-Trujillo, V. Lazic, J. Moros and J. J. Laserna, *Appl. Opt.*, 2017, **56**, 3773–3782.
68 N. Sharma, W. D. Bachalo and A. K. Agarwal, *Phys. Fluids*, 2020, **32**, 023304.
69 C. M. Gryniewicz-Ruzicka, S. Arzhantsev, L. N. Pelster, B. J. Westenberger, L. F. Buhse and J. F. Kauffman, *Appl. Spectrosc.*, 2011, **65**, 334–341.
70 M. Stobiecka and M. Hepel, *Phys. Chem. Chem. Phys.*, 2011, **13**, 1131–1139.
71 P. Rohilla and J. Marston, *Int. J. Pharm.*, 2020, **589**, 119714.
72 S. Mandato, E. Rondet, G. Delaplace, A. Barkouti, L. Galet, P. Accart, T. Ruiz and B. Cuq, *Powder Technol.*, 2012, **224**, 323–330.
73 J. Kohling and V. Wagner, *Int. J. Heat Mass Transfer*, 2021, **169**, 120939.
74 H. J. Jin, J. S. Chen, V. Karageorgiou, G. H. Altman and D. L. Kaplan, *Biomaterials*, 2004, **25**, 1039–1047.
75 B. L. Huang, T. L. Guo, S. Xu, Y. Ye, E. G. Chen and Z. X. Lin, *IEEE Photonics J.*, 2019, **11**, 1–9.
76 Z. Y. Hu, N. P. Bradshaw, B. Vanthournout, C. Forman, K. Gnanasekaran, M. P. Thompson, P. Smeets, A. Dhinojwala, M. D. Shawkey, M. C. Hersam and N. C. Gianneschi, *Chem. Mater.*, 2021, **33**, 6433–6442.
77 S. H. Lee, A. Mahadevegowda, C. Huang, J. D. Evans and P. S. Grant, *J. Mater. Chem. A*, 2018, **6**, 13133–13141.
78 B. H. Zhao, Y. B. Wang, S. Sinha, C. J. Chen, D. P. Liu, A. Dasgupta, L. B. Hu and S. Das, *Nanoscale*, 2019, **11**, 23402–23415.
79 A. Friederich, J. R. Binder and W. Bauer, *J. Am. Ceram. Soc.*, 2013, **96**, 2093–2099.
80 Y. Jang, Y. D. Park, J. A. Lim, H. S. Lee, W. H. Lee and K. Cho, *Appl. Phys. Lett.*, 2006, **89**, 183501.